Supplementary Information

Dual defect engineering tailored Li^+ diffusion kinetics for sustainable Mn-based composite-structure cathodes

Shiqi Liu[abc], Boya Wang[d], Shaoze Tian[abc], Bo Wang[e], Yulong Wang[abc], Zhaoyu Rong[e], Guanhua Zhang[f], Jinjin Zhang[g], Chenghan Li[abc], Tian Wang[abc], Ziliang Liu[abc], Xianwei Guo*[abch], Lin Gu*[d], Jianyu Huang[e] and Haijun Yu*[abc]

[a]Institute of Advanced Battery Materials and Devices, College of Materials Science and Engineering, Beijing University of Technology, Beijing 100124, China.

[b]Institute of Gongda-Guochuang Advanced Battery Materials and Devices, Beijing,100176, P. R. China.

[c]State Key Laboratory of Materials Low-Carbon Recycling, Institute of Matter Science, Beijing University of Technology, Beijing 100124, China.

[d]Beijing National Center for Electron Microscopy and Laboratory of Advanced Materials, School of Materials Science and Engineering, Tsinghua University, Beijing 100084, China.

[e]Clean Nano Energy Center, State Key Laboratory of Metastable Materials Science and Technology, Yanshan University, Qinhuangdao 066000, China.

[f]State Key Lab of Chemical Reaction Dynamics, Dalian Institute of Chemical Physics, Chinese Academy of Sciences, Dalian 116023, P.R. China.

[g]Shanghai Synchrotron Radiation Facility, Shanghai Advanced Research Institute, Chinese Academy of Sciences, Shanghai, China.

[h]Beijing Create Energy & Benefit Future Co., Ltd., Beijing 100176, China.

Corresponding author: Haijun Yu, Xianwei Guo, Lin Gu

E-mail: hj-yu@bjut.edu.cn, xwguo@bjut.edu.cn, lingu@mail.tsinghua.edu.cn

Methods

Preparation of Mn-based composite-structure cathode

The pristine Mn-LLO cathode was prepared by sintering the commercial Mn-based hydroxide precursor with the Li_2CO_3 (with 3 wt.% excess Li) under previously reported thermal processes procedures in the Create Energy & Benefit Future Co., Ltd. In the synthetic process, the Mn-based composite-structure cathode material was firstly prepared by mixing the Mn-LLO ($Li_{1.05}Mn_{0.52}Ni_{0.43}O_2$) with sandmilled $AlPO_4$ particles in a reasonable weight ratio (0.5, 1, and 2 wt.%) in the mechanofusion machine for 3 minutes. Then, the as-prepared composite-structure cathode was then heated at 900 ºC for 5 hours in the furnace. After this process, as-resulted cathode is labeled as Mn-LLO-AP.

Material characterization

Synchrotron X-ray diffraction experiments were performed at the BL02U2 beamline of the Shanghai Synchrotron Radiation Facility (SSRF, Shanghai). Cross-sectional microscopic measurements of the cathode particles were firstly performed using FIB-SEM (Helios G4 CX, Thermo Fisher Scientific) to obtain the nanometre-level thin film. Then the films were was transferred to a Spherical aberration-corrected electron microscopy (Titan, G2, 300 kV, Thermo Fisher Scientific) to harvest the high-angle annular dark-field (HAADF) atomic images and mapping images. The morphologies of as-prepared samples were observed by a field-emission scanning electron microscope (SEM, HITACHI SU8020). The X-ray photoelectron spectroscopy technique were performed on a Thermo ESCALAB 250Xi spectrometer. P K-edge XANES spectra were collected at the BL16U1 beamline of SSRF. The time-of-flight secondary ion mass spectrometry (TOF-SIMS) was performed using ION-TOF TOF-SIMS IV with a pulsed 30 keV gallium (Ga) liquid metal ion beam source and TESCAN S9000 scanning electronic microscopy equipped with FIB and TOF-SIMS accessories. The adsorption experiments were conducted using a BelCata II adsorption analyzer, and the evolved gases were analyzed with a BelMass mass spectrometer. The EPR spectra were recorded on a Bruke A300 spectrometer. The X-PEEM measurements were performed at BL09U (Dreamline) of the SSRF. O K-edge and Mn/Ni L-edge XAS measurements were performed at beamline MCD (BL10B and BL12B) at the National Synchrotron Radiation Laboratory (NSRL, Hefei).

Electrochemical measurements

The electrode films were prepared by coating the slurry consisting of the active material, Super P carbon, and polyvinylidene difluoride (PVDF) binder in a mass ratio of 8:1:1 onto the Al foil. And the mass loading of the active material was more than 6 mg cm^{-2}. After dried at 120 °C for 12 h in a vacuum, the obtained electrodes films were cut into pieces with a diameter of 10 mm and were assembled with the Celgard film as the separator and 1M $LiPF_6$ dissolved in ethylene carbonate (EC): ethyl methyl carbonate (EMC) (3:7 by volume) as the electrolyte into the CR2032 coin cell in the argon-filled glove box. The electrochemical performances were tested by the Neware battery test system (CT-4008Tn-5V10mA-164, Shenzhen, China) at 25 and 45 ºC.

The pouch cells were assembled by using double-faced active material coated electrode plates. The cathode was prepared by casting the slurry in the aluminum foil (active materials: PVDF:

carbon black = 92.5: 5: 2.5, in weight ratio). The graphite anode was prepared by 94 wt% active material, 1.5 wt% conductive agent, 3 wt% sodium carboxymethyl cellulose (CMC), and 1.5 wt% styrene-butadiene rubber binder (SBR). After drying, the cathode and anode sheets were cut into 4.3 × 5.6 cm and 4.5 × 5.8 cm, respectively. The 200 mAh pouch cells were processed with one layer of cathode and two layers of graphite anode. Finally, the pouch cells were sealed within a parched chamber after electrolyte injection, effectively managing the dew spots. The cells were tested at 25 °C using the NEWARE-CT4800Tn battery test system and the formation process involved cycling at the voltage range from 2.5 – 4.3 V at 0.1C, followed by cycling at 1C within the 2.5 to 4.3 V.

Theoretical calculations

All spin-polarized first-principles calculations were performed within the framework of density functional theory (DFT) as implemented in the Vienna Ab initio Simulation Package (VASP). The electron-ion interactions were described by the projector augmented-wave (PAW) method. The exchange-correlation functional was treated within the generalized gradient approximation (GGA) parameterized by Perdew, Burke, and Ernzerhof (PBE). The Brillouin zone was sampled at the Γ-point for 3a×3b×2c supercell. The effective Hubbard U parameters were set to 5.0 eV for Mn and 6.0 eV for Ni. The plane-wave basis set was expanded with a kinetic energy cutoff of 520 eV. Geometry optimizations were considered converged when the total energy change between successive electronic steps was less than 1×10^{-5} eV and the Hellmann-Feynman forces on all atoms were smaller than 0.01 eV/Å. The climbing image nudged elastic band (CI-NEB) method was used to locate the transition states and calculate the migration energy barriers.

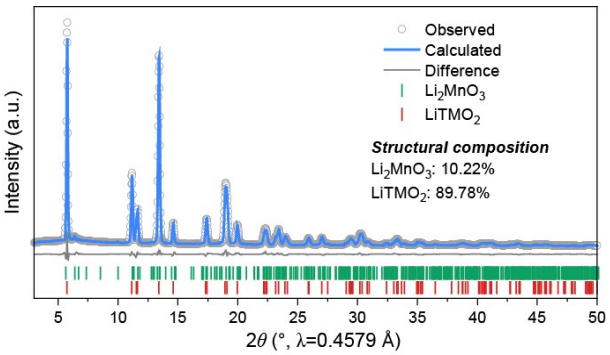

Fig. S1 | SXRD results of Mn-LLO cathode material.

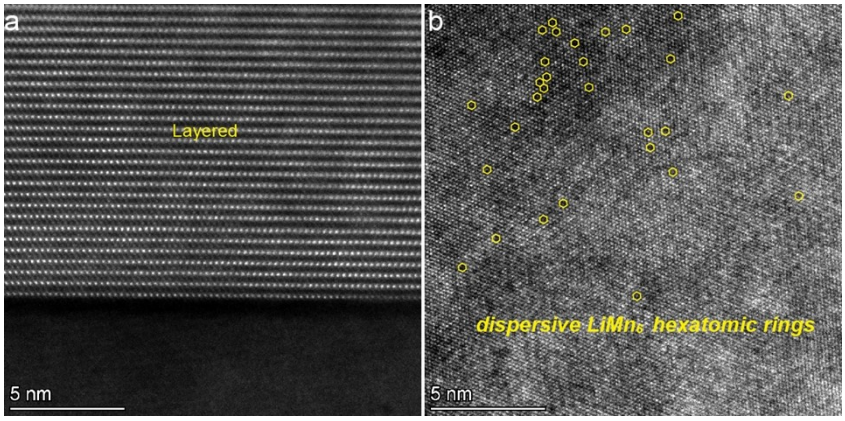

Fig. S2 | Additional HAADF-STEM images of Mn-LLO-AP cathode projected along the **a,** [100] zone axis and **b,** [001] zone axis. $LiMn_6$ hexatomic rings are highlighted by the yellow hexagon frames.

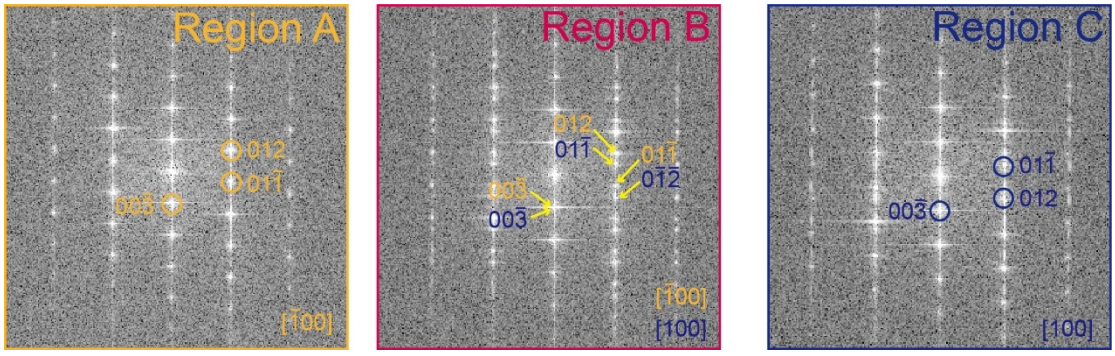

Fig. S3 | FFT patterns of selected regions of Mn-LLO-AP.

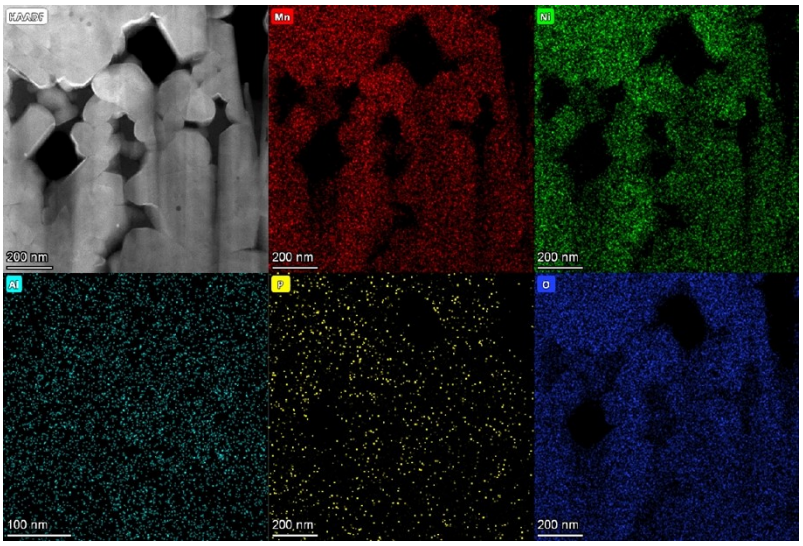

Fig. S4 | Additional EDS mapping results of Mn-LLO-AP collected under the TEM mode.

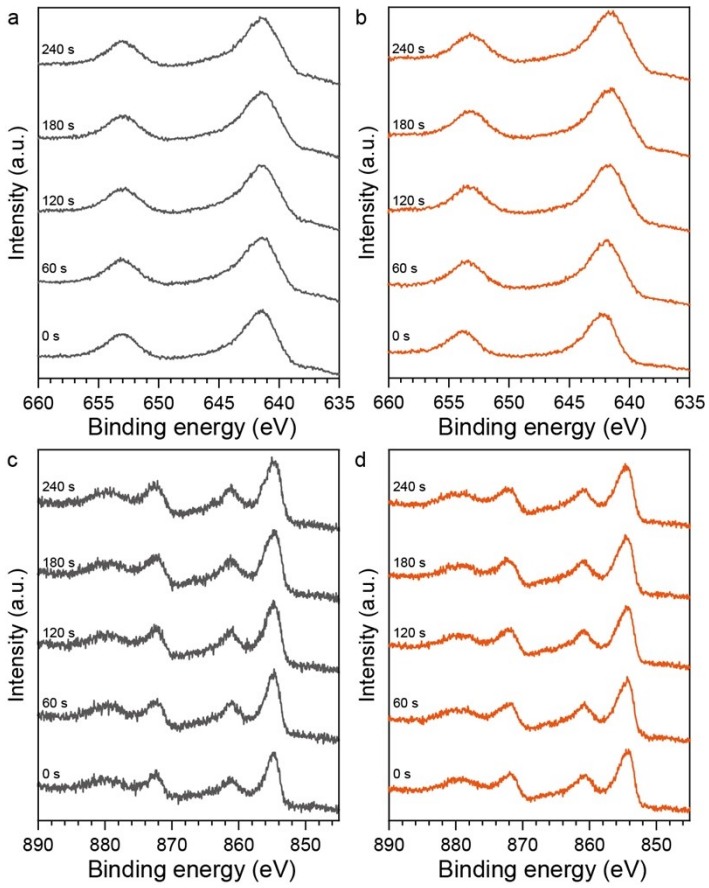

Fig. S5 | Mn 2p XPS spectra of **a,** Mn-LLO and **b,** Mn-LLO-AP and Ni 2p XPS spectra of **c,** Mn-LLO and **d,** Mn-LLO-AP with different Ar^+ sputtering times.

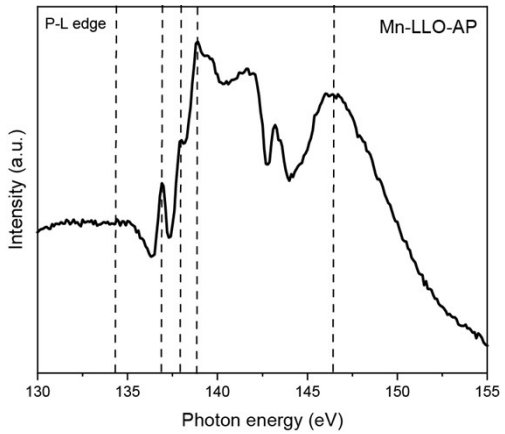

Fig. S6 | P L-edge SXAS spectrum of Mn-LLO-AP cathode.

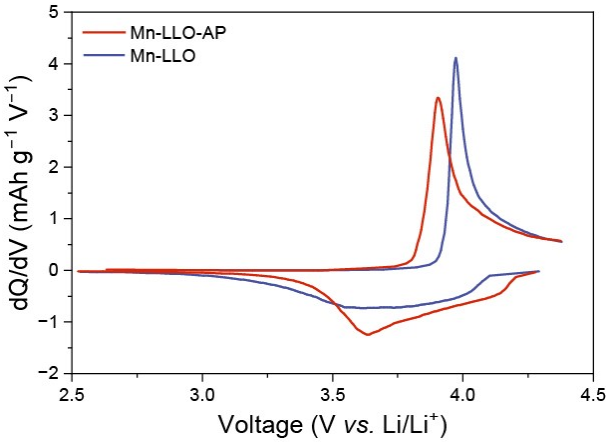

Fig. S7 | The initial cycle of dQ/dV plots at 1C for Mn-LLO and Mn-LLO-AP.

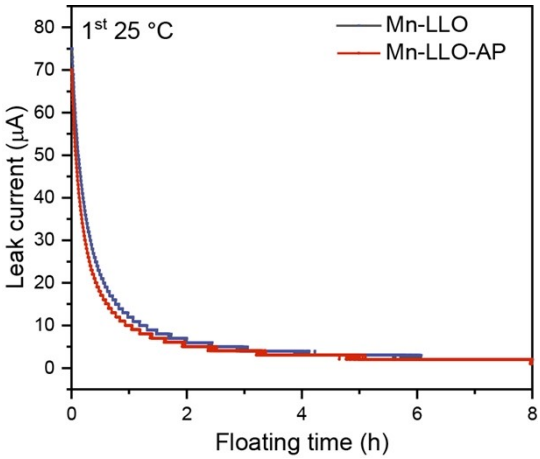

Fig. S8 | The leakage current during floating-charge tests collected from Mn-LLO and Mn-LLO-AP after the 1st cycle.

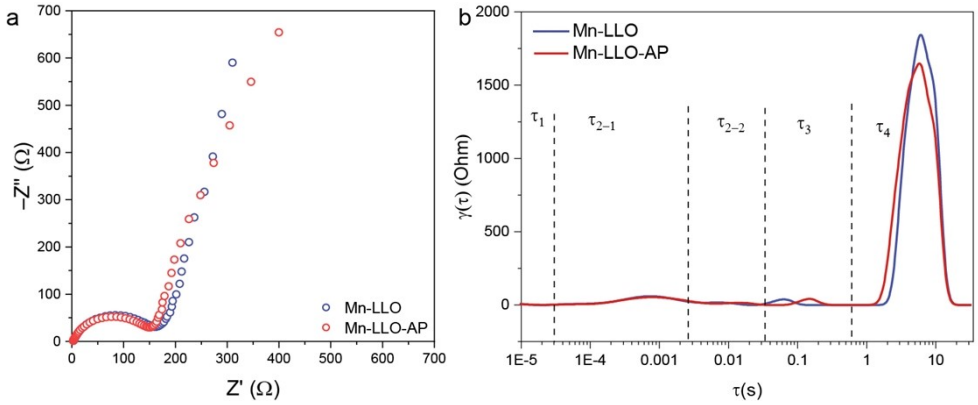

Fig. S9 | The **a,** EIS and **b,** DRT profiles of Mn-LLO and Mn-LLO-AP before electrochemical cycling.

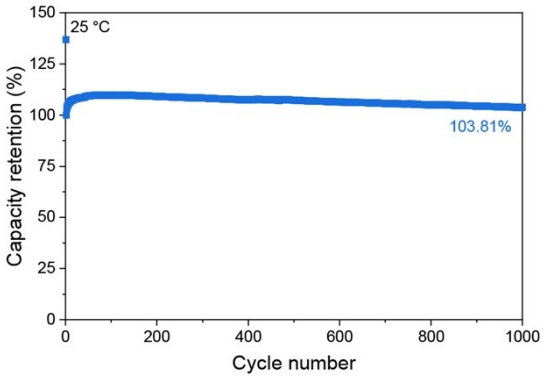

Fig. S10 | Cycle performance test at 25 °C in the 250 mAh pouch cell.

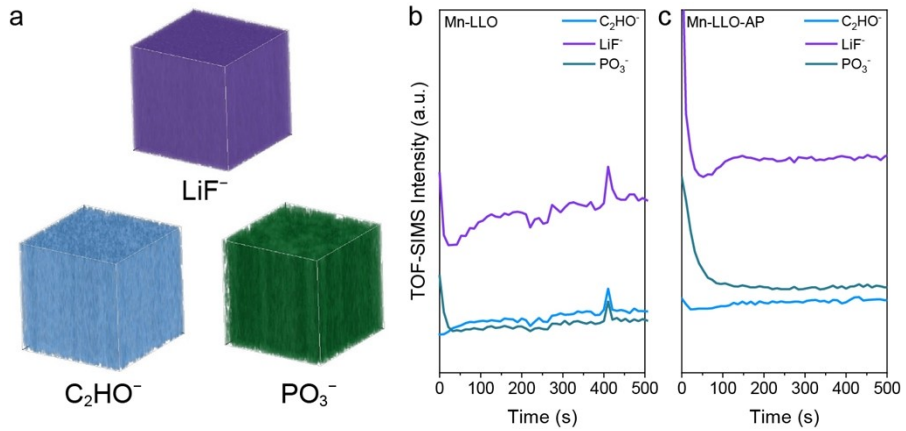

Fig. S11 | a, TOF-SIMS 3D rendering images of the LiF^-, C_2HO^-, and PO_3^- fragments of the Mn-LLO-AP electrode. **b,** Normalized depth profiles of representative fragments of TWO cathode materials after cycling.

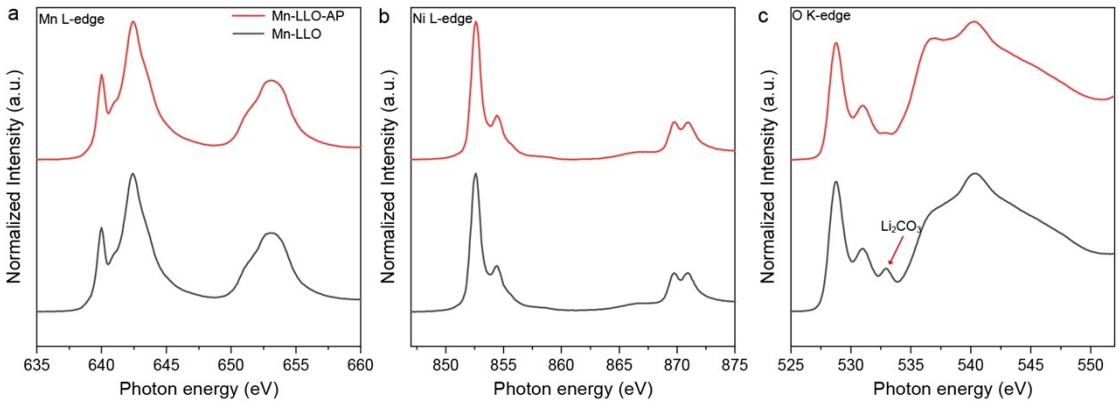

Fig. S12 | SXAS spectra collected at the photon energy of **a,** Mn L-edge **b,** Ni L-edge and **c,** O K-edge of Mn-LLO and Mn-LLO-AP at the pristine state.

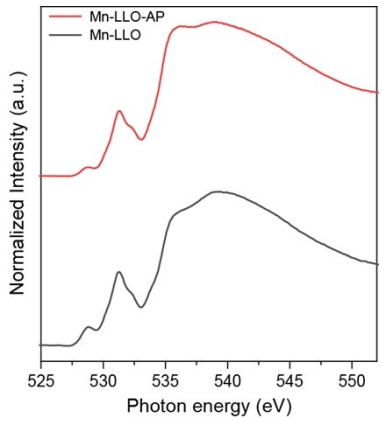

Fig. S13 | SXAS spectra collected at the photon energy of O K-edge of Mn-LLO and Mn-LLO-AP after 400 cycles.

Table S1 | SXRD refinement results of Mn-LLO.

Site	Wyckoff position	*x*	*y*	*z*	Occupation	B_{iso}
Mn1	4g	0	0.176	0	0.263(1)	0.111
Li1	4g	0	0.176	0	0.737(1)	0.111
Li2	2b	0	0.5	0	0.958(1)	0.111
Mn2	2b	0	0.5	0	0.042(1)	0.111
Li3	2c	0	0	0.5	1	0.149
Li4	4h	0	0.730	0.5	1	0.149
O1	4i	0.141	0	0.121	1	0.333
O2	8j	0.212	0.320	0.203	1	0.333
Phase Li_2MnO_3, a=4.9210(1) Å; b=8.541(2) Å; c=5.1342(2) Å; β=110.16(3)°, V = 202.59(1) Å^3, fraction: 10.22%						
Site	Wyckoff position	*x*	*y*	*z*	Occupation	
Li_1	3b	0.000	0.000	0.000	0.939(3)	0.149
Ni_1	3b	0.000	0.000	0.000	0.060(7)	0.149
Ni_2	3a	0.000	0.000	0.500	0.439(3)	0.111
Li_2	3a	0.000	0.000	0.500	0.060(7)	0.111
Mn	3a	0.000	0.000	0.500	0.5	0.111
O	6c	0.000	0.000	0.241(1)	1	0.333
Phase $LiMn_{0.5}Ni_{0.5}O_2$, a=2.86933(1) Å, c=14.2226(9) Å, V=101.407(1) Å^3, fraction: 89.78%						

Table S2 | SXRD refinement results of Mn-LLO-AP.

Site	Wyckoff position	*x*	*y*	*z*	Occupation	B_{iso}
Mn1	4g	0	0.176(1)	0	1	0.111
Li2	2b	0	0.5	0	1	0.111
Li3	2c	0	0	0.5	1	0.149
Li4	4h	0	0.730	0.5	1	0.149
O1	4i	0.239(4)	0	0.197(6)	1	0.333
O2	8j	0.307(2)	0.299(3)	0.836(4)	1	0.333
Phase Li_2MnO_3, a=4.954(3) Å; b=8.538(3) Å; c=5.0766(1) Å; β=107.871(1)°, V = 204.37(9)Å^3, fraction: 10.19%						
Site	Wyckoff position	*x*	*y*	*z*	Occupation	
Li_1	3b	0.000	0.000	0.000	0.918(5)	0.149
Ni_1	3b	0.000	0.000	0.000	0.081(5)	0.149
Ni_2	3a	0.000	0.000	0.500	0.418(5)	0.111
Li_2	3a	0.000	0.000	0.500	0.081(5)	0.111
Mn	3a	0.000	0.000	0.500	0.50	0.111
O	6c	0.000	0.000	0.240(9)	0.94	0.333
Phase $LiMn_{0.5}Ni_{0.5}O_2$, a=2.8792(1) Å, c=14.2747(7) Å, V=102.481(8) Å^3, fraction: 89.81%						

Table S3 | NPD refinement results of Mn-LLO-AP.

Site	Wyckoff position	*x*	*y*	*z*	Occupation	U_{iso}
Li_1	3b	0.000	0.000	0.000	0.973(3)	0.0285
Ni_1	3b	0.000	0.000	0.000	0.026(7)	0.0285
Ni_2	3a	0.000	0.000	0.500	0.403(3)	0.03453
Li_2	3a	0.000	0.000	0.500	0.076(7)	0.03453
Mn	3a	0.000	0.000	0.500	0.520	0.03453
O	6c	0.000	0.000	0.242(1)	0.940	0.00931
a=2.8835(8) Å, c=14.317(2) Å, V=103.099(1) Å^3						